Sensors and Materials, Vol. 34, No. 12 (2022) 4425–4434
MYU Tokyo

S & M 3119

Two Different Layouts of Sensors of Four-gauge Borehole Strainmeter and Their Influence on Field Measurement

Lei Tang,[1*] Junyi Fan,[1] Miao Miao,[2] and Zheng Chen[3]

[1]China Earthquake Networks Center, China Earthquake Administration, Beijing 100045, China
[2]Department of Earth and Space Sciences, Southern University of Science and Technology, Shenzhen 518055, China
[3]National Institute of Natural Hazards, Ministry of Emergency Management of China, Beijing 100085, China

(Received October 22, 2022; accepted November 16, 2022; online published December 5, 2022)

Keywords: four-gauge borehole strainmeter, self-consistent, layout mode, numerical simulation

The four-gauge borehole strainmeters (FGBSs) used in mainland China include multiple instrument modes. The sensors in the four directions have two layout modes in the vertical direction: the same-plane mode and the different-plane mode. In this study, we obtained a large amount of site observation data and showed that the observation data collected using the two modes have certain differences. Through the establishment of a 3D finite element model and field measurement analysis, it was concluded that the inhomogeneity of the coupling cement at different levels influenced the observations of the sensors in the different-plane mode, and the observation data were less self-consistent than those for instruments with sensors in the same-plane mode. The self-consistent characteristics of the FGBS provide an algorithm for AI-based seismic research. Comprehensive analysis showed that for the four sensors of the FGBS, the same-plane layout was the optimal choice.

1. Introduction

Since the 1960s, borehole strainmeters have been used to conduct deformation observations to study the characteristics of crustal deformation and stress field changes in dozens of countries and regions, including the United States,[1–3] Japan,[4] and China.[5–7] This method has been used to study plate movements, earthquakes, volcanoes, and many other geological phenomena.[8–15]

Previous borehole strainmeters used in mainland China include volumetric strainmeters and four-gauge borehole strainmeters (FGBSs).[5–7] An FGBS is generally installed in a borehole in bedrock at a depth of tens or hundreds of meters to observe changes in the horizontal strain in the shallow surface of the crust. Figure 1 shows a schematic diagram of the overall composition of a standard borehole strain observation system. The probe of the FGBS is a sealed steel cylinder with a circular cross section and a sensor for measuring changes in the inner diameter. The instrument probe is placed in the borehole at a location with a hard and complete rock texture, and the space between the probe and the surrounding medium is filled with coupling cement (a mixture of cement and quartz sand prepared in a specific proportion according to the

*Corresponding author: e-mail: TangLei06@seis.ac.cn
https://doi.org/10.18494/SAM4186

ISSN 0914-4935

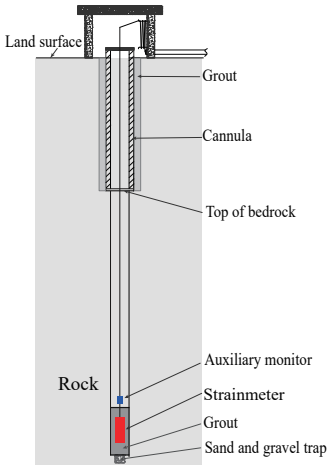

Fig. 1. (Color online) Overall composition of a standard borehole strain observation system.

rock properties of the measured section), coupling the instrument probe with the rock. Auxiliary monitors such as a thermometer, barometer, and water level gauge are installed above the strain probe, the measurements of which are compared with the strain observations to facilitate analysis of the observation data and to eliminate the interference of the observation environment. In addition, the casing is placed from the drilling wellhead to the top of the bedrock, and cement is used to fill the space between the casing and the hole wall to ensure the quality of the observation hole and to prevent a collapse of the hole wall.

2. Theoretical Model and Observation Principle

Consistent with the component borehole tensor strainmeters used in Japan, the United States, and other countries,[2–4,16] when there are uniform horizontal principal strains ε_1 and ε_2 in the section of the formation near the borehole, the components installed in the borehole along the θ direction directly observe the relative change in the inner diameter of the probe sleeve in this direction S_θ; that is, the ratio of the change in the length of the component to the length of the component. The theoretical formula for S_θ is as follows:

$$S_\theta = A(\varepsilon_1 + \varepsilon_2) + B(\varepsilon_1 - \varepsilon_2)\cos 2(\theta - \varphi), \tag{1}$$

where φ is the azimuthal angle of ε_1, and A and B are two parameters that need to be determined.

As shown in Fig. 2(a), there are four horizontally arranged sensors in the probe of an FGBS. The angle between the two gauges is 45°, and the relative changes in the aperture in the four directions are measured.[13] According to Eq. (1), the measurements of the four gauges are expressed as follows:

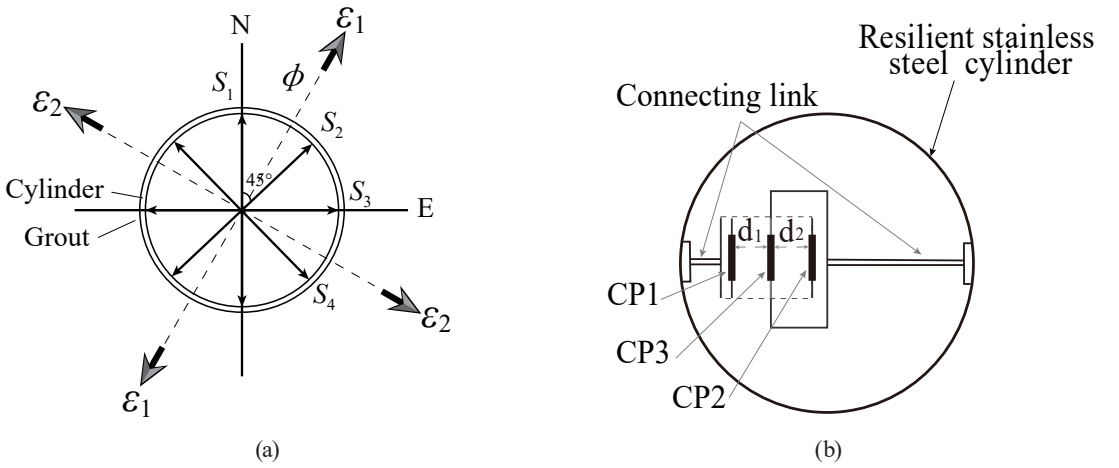

Fig. 2. (a) Schematic diagram of a standard borehole strainmeter. S_1, S_2, S_3, and S_4 are the sensors in the four directions, and ε_1 and ε_2 are the maximum and minimum principal strains, respectively. (b) Cross section of FGBS strain gauge. CP1, CP2, and CP3 are the three capacitor plates, d1 is the gap between CP1 and CP3, and d2 is the gap between CP2 and CP3.

$$\begin{cases} S_1 = S_{\theta_1} = A(\varepsilon_1 + \varepsilon_2) + B(\varepsilon_1 - \varepsilon_2)\cos 2(\theta_1 - \varphi), \\ S_2 = S_{\theta_1 + \pi/4} = A(\varepsilon_1 + \varepsilon_2) - B(\varepsilon_1 - \varepsilon_2)\sin 2(\theta_1 - \varphi), \\ S_3 = S_{\theta_1 + \pi/2} = A(\varepsilon_1 + \varepsilon_2) - B(\varepsilon_1 - \varepsilon_2)\cos 2(\theta_1 - \varphi), \\ S_4 = S_{\theta_1 + 3\pi/4} = A(\varepsilon_1 + \varepsilon_2) + B(\varepsilon_1 - \varepsilon_2)\sin 2(\theta_1 - \varphi), \end{cases} \tag{2}$$

where θ_1 is the azimuth of gauge 1.

Using Eq. (2), we can obtain the following simple and important relation:

$$S_1 + S_3 = S_2 + S_4 = 2A(\varepsilon_1 + \varepsilon_2)\,, \tag{3}$$

where $S_1 + S_3$ and $S_2 + S_4$ are two sets of observed plane strains. The relationship expressed in Eq. (3) is called the self-consistency equation of the FGBS, in which θ_1 is arbitrary, in that the relationship is independent of the azimuth angle of the element.[15] For any two mutually perpendicular components, their sum is a constant value. This indicates the correlation expected between the measured values in the four directions. Although this self-consistency equation is simple, it is the most significant characteristic of an FGBS and an important index used to judge whether its installation has been successful. It also provides an algorithm for AI-based seismic research.

For each FGBS sensor, a three-electrode differential capacitance sensor is used to reflect the deformation of the probe housing by measuring the differential change in the capacitance. As shown in Fig. 2(b), the three plates (CP1, CP2, and CP3) remain parallel. Plates CP1 and CP2 on both sides are fixed on the cylinder wall in the opposite direction of the diameter to ensure that the spacing is fixed, the middle plate CP3 can move, the spacing between plates CP1 and CP3 is

d_1, and the spacing between plates CP2 and CP3 is d_2. The change in the borehole diameter causes radial displacement of the outer wall of the probe, and d_1 and d_2 change accordingly, but the sum of d_1 and d_2 is a fixed constant. The distance between the plates changes, and the capacitance changes accordingly. The measurement circuit converts the capacitance change into a voltage value and sends it to the ground through a signal cable. The relationship between the voltage value and the strain value output by each component measured in the laboratory is converted into a strain value.

3. Layouts of Sensors

At present, there are many types of FGBS instruments.[5,6,16] Owing to their different production processes, the layouts of the four sensors of the different types of instruments are different, but their layouts can be divided into two basic types: the four sensors are in the same-plane mode [Fig. 3(a), defined as mode A in this paper] and the different-plane mode [Fig. 3(b), defined as mode B]. The maximum vertical interval between two adjacent gauges in the known mode B instruments is 10 cm, and the maximum distance between the four sensor components is 30 cm. In theory, under the conditions of a uniform rock medium, uniform ground stress, and a drilling depth of tens to hundreds of meters, mode B can also be approximated as the same-plane observation.

The two layout modes of the sensor gauges lead to different overall lengths of the instrument probe, and they also lead to different installation methods. We take the YRY-4-type FGBS as a representative of mode A and the RZB-type FGBS as a representative of mode B as examples, Figure 4 presents schematic diagrams of the probe bodies and sensor gauges of the two types of FGBS.[5,6] For the YRY-4-type FGBS, the probe body is 400 mm long, the probe diameter is 107 mm, and, to avoid the influence of the surface temperature, a suitable installation depth is about 30–60 m. The probe body and sensor gauge structure are shown in Fig. 4(a). For the RZB-type FGBS, the probe body is 1100 mm long, the outer diameter of the probe is 102 mm, and a suitable installation depth is 60–300 m. The structure of the probe body and the sensor element are

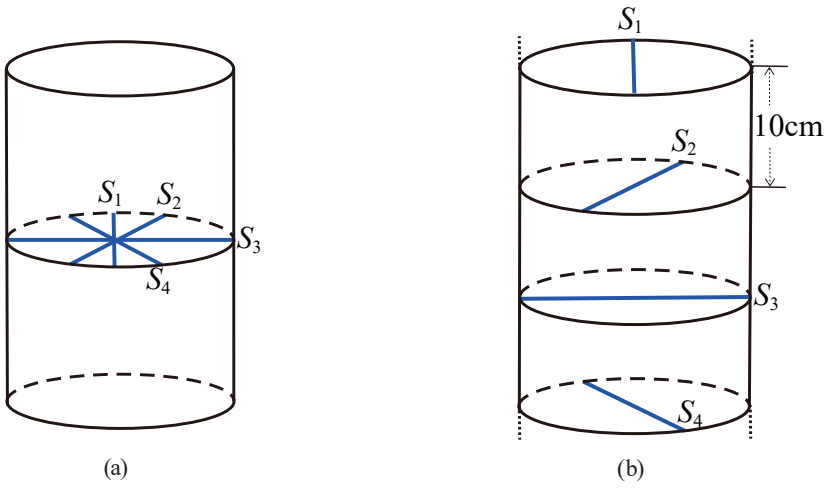

Fig. 3. (Color online) Two layout modes of sensors for FGBS. (a) Mode A. (b) Mode B.

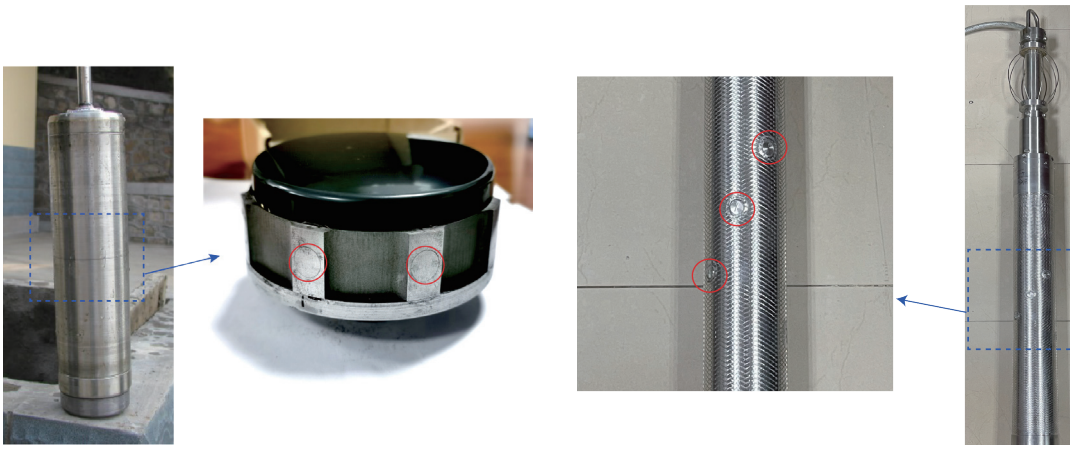

(a) (b)

Fig. 4. (Color) (a) YRY-4-type FGBS probe body and sensor gauge. (b) RZB-type FGBS probe body and sensor gauge. The blue box shows the position of the probe where the sensor is located, and the red circles represent the positions of the sensor gauges.

shown in Fig. 4(b). The overall length and weight of the YRY-4-type FGBS probe are small, making it easy to install, and it can be installed without the need for extra equipment. Owing to the long main body and heavy weight of other probes, the RZB-type FGBS must be fixed with a tripod to assist in the installation. The top of the tripod uses a fixed pulley to guide the wire rope. The strain probe is connected to the wire rope through the upper lifting beam, and the winch controls the lowering of the probe. At present, there are 41 YRY-4 sites and 27 RZB sites in the borehole strain network in mainland China.

4. Results and Discussion

FGBSs of both modes were installed in boreholes with depths of tens to hundreds of meters. The rock around the probe was hard and complete, and the medium and geological conditions were regarded as homogeneous. Therefore, in theory, under the condition that the rock properties, installation depth, and coupling conditions are consistent, the changes in strain observed by the two modes should be consistent. The observation results should also conform to the self-consistency equation [e.g., Eq. (3)], that is, $S_1 + S_3 = S_2 + S_4$. However, the observation results for a large number of stations revealed some differences between the two modes. To explore the reasons for these differences, we used the field measurements to establish a 3D finite element model (FEM) for comprehensive analysis.

4.1 Field measurements

In this paper, the self-consistency of the observation data for the two modes was analyzed on the basis of field measurements collected using a YRY-4-type FGBS in the Gaotai (GT) site in Gansu Province and an RZB-type FGBS in the Kumish (KMS) site in Xinjiang Province. Figure

5 shows the time series curves of $S_1 + S_3$ and $S_2 + S_4$ for different time scales, which qualitatively show the correlation between $S_1 + S_3$ and $S_2 + S_4$. Among them, Figs. 5(a) and 5(b) show the correlation between $S_1 + S_3$ and $S_2 + S_4$ on a short-term scale (i.e., from Jan 1, 2021 to Jan 10, 2021) for the GT (mode A) and KMS (mode B) sites, respectively. The two curves in Fig. 5(a) almost overlap, the correlation coefficient between them is 0.9998, and the changes in the amplitude of the data are also consistent. The consistency of the two curves shown in Fig. 5(b) is slightly lower and the correlation coefficient is slightly smaller, but it is still as high as 0.9913. However, the changes in the amplitude of the data are basically the same. Figures 5(c) and 5(d) show the correlation between $S_1 + S_3$ and $S_2 + S_4$ on a long-term scale (i.e., from Jan 1, 2021 to Dec 31, 2021). The two curves in Fig. 5(c) almost overlap, the correlation coefficient is 0.9991, and the changes in the amplitude data are consistent. The correlation coefficient of the two curves in Fig. 5(d) is 0.9881. Figure 5(d) also shows greater dispersion of the two curves and a larger difference in the relative change in the data over time.

According to the above methods and results, we analyzed the best 10 sites for the two modes on a long-term scale (i.e., from Jan 1, 2021 to Dec 31, 2021). As shown in Table 1, the mean correlation coefficient of the 10 sites for mode A is 0.9928 and that for mode B is 0.9821. On the basis of these results, the characteristics of the two modes of FGBSs were obtained. The observations recorded using the two modes indicated a clear solid strain tide, but tidal calibration should be performed when using these data.[16,17] For mode A, the observation data have high

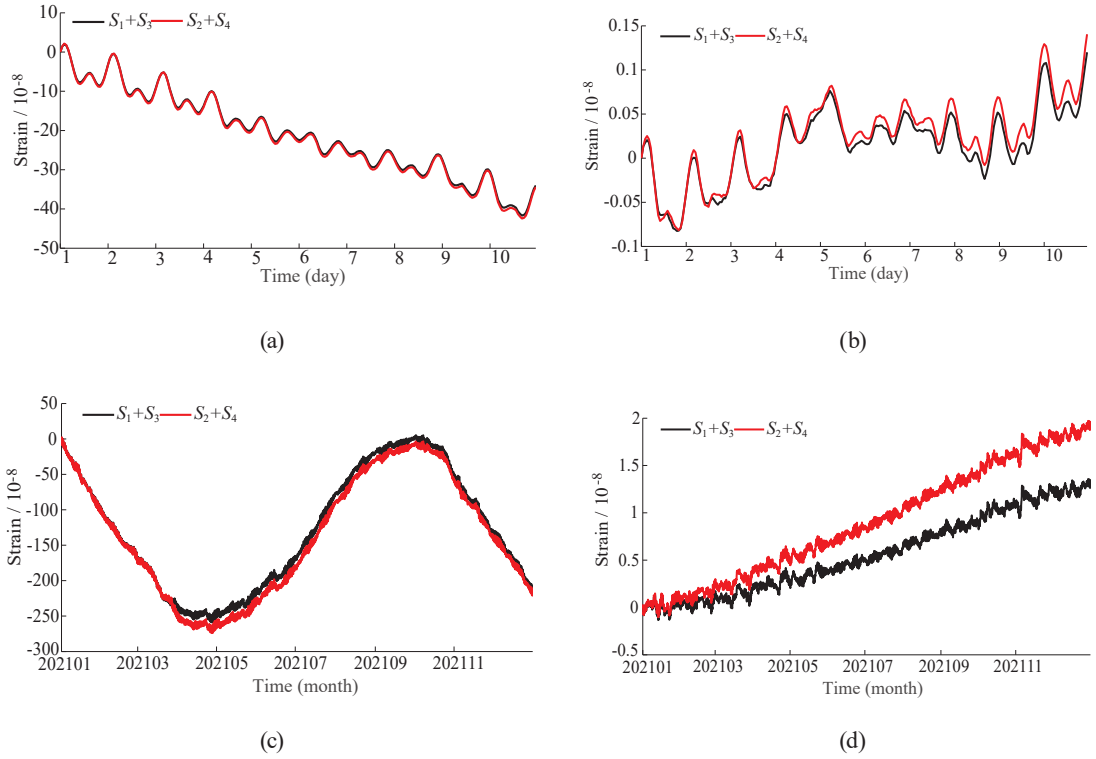

Fig. 5. (Color) Measured time series curves of $S_1 + S_3$ and $S_2 + S_4$ for different time scales. (a) Short-term scale curves of mode A. (b) Short-term scale curves of mode B. (c) Long-term scale curves of mode A. (d) Long-term scale curves of mode B.

Table 1
Correlation coefficient values of 10 best sites for two modes.

Mode A	Sites	SS	GT	ZT	HY	YP	JH	NSK	DLH	SC	CS
	Value	0.9994	0.9991	0.9958	0.9955	0.9914	0.9914	0.9905	0.9904	0.9893	0.9854
Mode B	Sites	SZHS	ZC	BNSL	BX	KMS	QD	MY	DJXM	BL	TA
	Value	0.9988	0.9983	0.9966	0.9894	0.9881	0.9868	0.9718	0.9716	0.9676	0.9521

self-consistency and fully satisfy the self-consistent equation on both the short-term and long-term time scales. For mode B, the self-consistency of the observation data is lower for the long time scale, and the relative variation of the amplitude of the strain on the two observation surfaces is also markedly different, which may be related to the sensor layout. When the sensors are arranged on the same plane, the medium at the position of the four gauges is uniform; however, when the sensors are arranged on different planes, a vertical distance of at least 30 cm is required, and the medium at the positions of the four gauges is not uniform.

4.2 Numerical simulation analysis

To study the self-consistency of the FGBSs with the two modes under a uniform rock medium and uniform in situ stresses, we created a 3D FEM with dimensions of 100 m × 100 m × 100 m based on the structure of the borehole strain-recording system. To avoid the boundary effect, the borehole was placed in the center of the model. The FEM was meshed into 13312 first-order hexahedral elements and 1122376 tetrahedral elements, and the characteristic length of the element was 0.005 m near the borehole and increased to 2 m near the boundaries (Fig. 6).

The basic assumptions were as follows. (1) On the 1-year time scale, a maximum horizontal principal stress of σ_1 = 1 kPa and a minimum horizontal principal stress of σ_2 = 0.6 kPa were applied to the eastern and northern boundaries of the model, respectively. As the time scale increased, the southern and western boundaries were constrained vertically, and the bottom of the model was constrained vertically. (2) The elastic moduli E and Poisson's ratios v of the rock, cement, and steel cylinder were defined. The range of E was 1–10 × 10^{10} Pa and the range of v was 0.15–0.35. (3) Strains e_1, e_2, e_3, and e_4 were the strains of the FGBS at different depths in the north–south, north–east, east–west, and south–east directions, respectively, with a 45° angle.

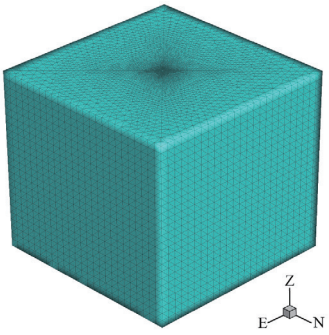

Fig. 6. (Color) 3D FEM of the borehole.

Under the various conditions of the above assumptions, the changes in the two sets of plane strains ($e_1 + e_3$ and $e_2 + e_4$) on different time scales and under different conditions were calculated, and the results were found to be basically the same.[18] Taking the 1-year time scale as an example, the constraints of $\sigma_1 = 1$ kPa, $\sigma_2 = 0.6$ kPa, $E = 4.5 \times 10^{10}$ Pa, and $\nu = 0.3$ were set. As shown in Fig. 7, the correlation coefficients between $e_1 + e_3$ and $e_2 + e_4$ for the two modes were equal to 1, and the trends in the change and the amplitude were very similar [Figs. 7(a) and 7(b)]. Because the strain was a relative change, the simulated strain values [Figs. 7(a) and 7(b)] were subtracted from the initial value to obtain Figs. 7(c) and 7(d). The results show that the relative change curves of $e_1 + e_3$ and $e_2 + e_4$ are almost coincident.

The numerical simulation results revealed that the FGBS was completely self-consistent for a uniform rock medium and uniform in situ stress, and the rock properties and measurement depth had little effect on the self-consistency of the FGBS.

4.3 Case study

Through analysis of the measurements and 3D FEM simulation results, it was found that for a uniform rock medium and uniform in situ stress, the simulation results were consistent with the theoretical relationships, and the results of the two sensor gauge layout modes were completely

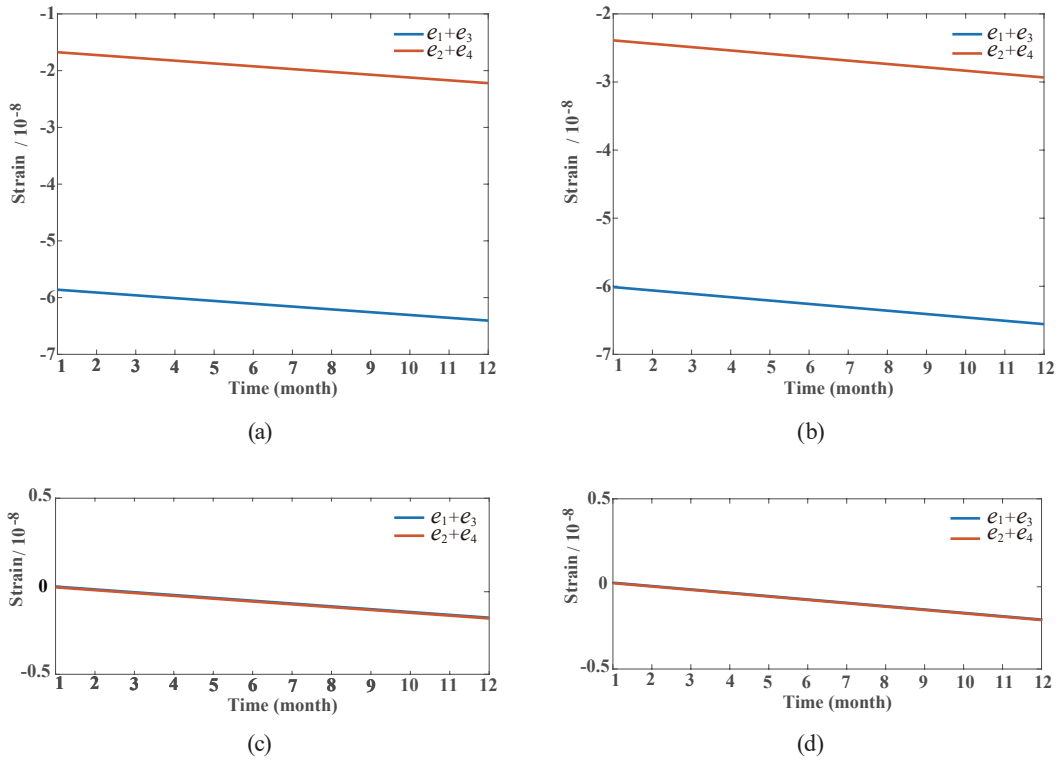

Fig. 7. (Color) Two groups of plane strain and relative change in plane strain curves of two modes of numerical simulation. (a) Plane strain curves of mode A. (b) Plane strain curves of mode B. (c) Curves showing relative change in plane strain of mode A. (d) Curves showing relative change in plane strain of mode B.

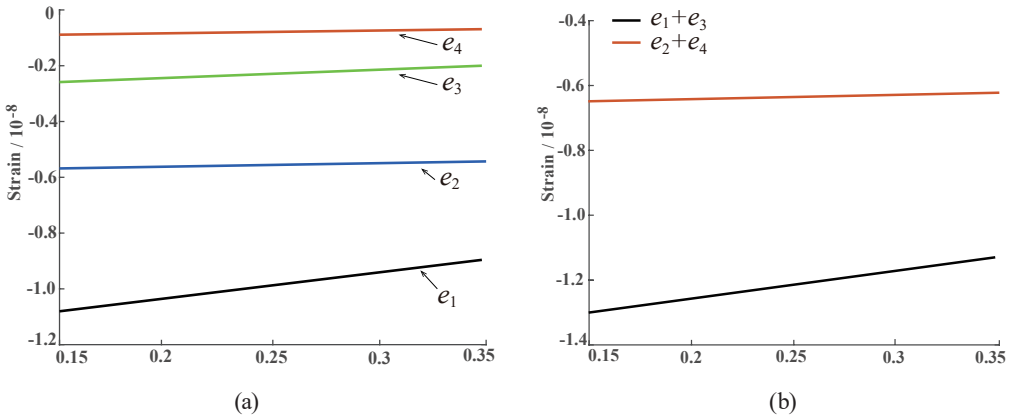

Fig. 8. (Color) Effects of the Poisson's ratio of the cement on (a) component strain and (b) two groups of plane strain.

consistent with the self-consistency equation. However, a large number of measurements showed that the self-consistency of the observation data produced by the FGBS with the sensor gauges arranged in the same-plane mode was better than that of the FGBS with the sensor gauges arranged in the different-plane mode.

On the basis of the numerical simulation analysis of the factors influencing the borehole strain observations,[18] several conclusions were obtained by using the 3D FEM established in this paper to simulate the influences of the rock, coupling cement, elastic modulus of the probe, and Poisson's ratio on the component strain and plane strain observations. First, the section measured by the probe was generally at least twice the length of the probe and was a complete section of rock with a hard texture, which was selected on the basis of rock coring and downhole TV. This basically ensured that the rock medium in the measuring section was uniform. Second, the steel cylinder of the probe was constructed of high-quality steel, and the steel cylinder was a homogeneous medium. Third, the change in the Poisson's ratio of the coupling cement had a major influence on the component strain and plane strain [Figs. 8(a) and 8(b)], and the possibility of inhomogeneity of the cement medium at different levels was the main reason for this. This led to the Poisson's ratio of the cement at the levels of the four components being different, which resulted in the two groups of plane strain $e_1 + e_3$ and $e_2 + e_4$ being different.

Through our research and analysis, it was concluded that the cement had a medium degree of inhomogeneity at different levels. This occurred because the cement and quartz sand could not be completely uniformly mixed. Second, the cement could not be consolidated at the same time at different levels. These factors may be the main reasons for the differences between the two groups of plane strains $S_1 + S_3$ and $S_2 + S_4$ for the different-plane mode of the sensor gauges.

5. Conclusions

In this study, we analyzed two sensor gauge layouts of FGBSs used in mainland China from the aspects of theoretical principles, 3D finite element numerical models, and field measurements. The results revealed that because the cement and quartz sand could not be

completely uniformly mixed and because the cement at different levels could not be consolidated at the same time, there was a creep effect and a medium degree of inhomogeneity of the cement at different levels. These factors made the self-consistency of the observation data for the different-plane mode of the sensor gauges slightly lower than that of the same-plane mode. The time series curves of the two sets of observation plane strain data gradually diverged, and the relative variation amplitudes were markedly different. Thus, it was concluded that to eliminate the influence of the inhomogeneity of the cement at different levels in multi-component borehole strainmeter measurements, the sensor gauges of the multi-component borehole strainmeter should be arranged in the same plane.

Acknowledgments

This work was supported by the National Natural Science Foundation of China (Grant No. 41974018) and a research grant (Grant No. ZDJ2018-09) from the National Institute of Natural Hazards, Ministry of Emergency Management of China. We acknowledge Mr. Shunliang Chi for providing the sensor images of the YRY-4-type FGBS. We thank LetPub (www.letpub.com) for its linguistic assistance during the preparation of this manuscript.

References

1 K. I. S. Sacks, S. Suyehiro, and D. W. Evertson: Proc. Jpn. Acad. **47** (1971) 70. https://doi.org/10.2183/pjab1945.47.707
2 M. T. Gladwin: Rev. Sci. Instrum. **55** (1984) 2011. https://doi.org/10.1063/1.1137704
3 M. T. Gladwin and R. Hart: Pure Appl. Geophys. **123** (1985) 59. https://doi.org/10.1007/BF00877049
4 H. Ishii: Report of Tono Research Institute of Earthquake Science **6** (2001) 5 (in Japanese).
5 K. Z. Su: Seismolog. Res. **4** (1982) 57 (in Chinese).
6 Z. X. Ouyang, Z. R. Zhang, and G. L. Shu: Chin. J. Rock Mech. Eng. **23** (2004) 4058 (in Chinese). https://doi.org/10.3321/j.issn:1000-6915.2004.23.025
7 S. L. Chi, Y. Chi, T. Deng, C. W. Liao, X. L. Tang, and L. Chi: Recent Dev. World Seismolog. **1** (2009) 1 (in Chinese).
8 A. Canitano, M. Mouyen, Y. Hsu, A. Linde, S. Sacks, and H. Lee: GeoHazards. **2** (2021) 172. https://doi.org/10.3390/geohazards2030010
9 A. T. Linde, M. T. Gladwin, M. J. S. Johnston, R. L. Gwyther, and R. G.Bilham: Nature **383** (1996) 65. https://doi.org/10.1038/383065a0
10 A. Canitano, Y. J. Hsu, H. M. Lee, A. T. Linde, and S. Sacks: J. Geod. **91** (2017) 1. https://doi.org/10.1007/s00190-016-0933-6
11 A. J. Barbour, J. O. Langbein, and N. S. Farghal: Bull. Seismol. Soc. Am. **111** (2021) 1325. https://doi.org/10.1785/0120200360
12 F. K. Wyatt, D. C. Agnew, and M. T. Gladwin: Bull. Seismol. Soc. Am. **84** (1994) 768. https://doi.org/10.1785/BSSA0840030768
13 G. Currenti, L. Zuccarello, A. Bonaccorso, and A. Sicali: J. Geophys. Res.: Solid Earth. **122** (2017) 7729. https://doi.org/10.1002/2017JB014663
14 Y. J. Li, H. P. Zhan, L. Tang, L. W. Chen, and Y. Jing: Front. Earth Sci. **8** (2020) 588304. https://doi.org/10.3389/feart.2020.588304
15 Z. Gong, Y. Jing, H. B. Li, L. Li, X. Y. Fan, and Z. Liu: J. Asian Earth Sci. **183** (2019) 103958. https://doi.org/10.1016/j.jseaes.2019.103958
16 Z. H. Qiu, L. Tang, B. H. Zhang, and Y. P. Guo: J. Geophys. Res.:Solid Earth. **118** (2013) 1609. https://doi.org/10.1002/jgrb.50112
17 E. Roeloffs: J. Geophys. Res.: Solid Earth. **115** (2010) B6. https://doi.org/10.1029/2009JB006407.
18 Y. J. LI, Y. Z. Lu, L. W. Chen, Z. M. Zhan, and J. Y. Ye: J. Geod. Geodyn. **31** (2011) 34 (in Chinese).